Optical Properties of Femtosecond Laser-Synthesized Silicon Nanoparticles in Deionized Water

ARTICLE *in* THE JOURNAL OF PHYSICAL CHEMISTRY C · MARCH 2011

Impact Factor: 4.77 · DOI: 10.1021/jp109351t

THE JOURNAL OF PHYSICAL CHEMISTRY C

ARTICLE

pubs.acs.org/JPCC

Optical Properties of Femtosecond Laser-Synthesized Silicon Nanoparticles in Deionized Water

R. Intartaglia,*[,†] K. Bagga,[†] F. Brandi,[†] G. Das,[†] A. Genovese,[†] E. Di Fabrizio,[†,‡] and A. Diaspro[†]

[†]Italian Institute of Technology (IIT), via Morego 30, 16152 Genoa, Italy

[‡]BIONEM lab, University Magna Graecia, Viale Europa Catanzaro, Italy

ABSTRACT: Silicon nanoparticles were prepared by ultrafast laser ablation of a silicon target in deionized water. The nanoparticles were characterized by using optical absorption, Raman spectroscopy, and transmission electron microscopy. The mean size is found to vary from 60 to 2.5 nm in the absence of any reducing chemical reagents, decreasing the pulse energy value. High-resolution transmission electron microscopy together with Raman spectroscopy confirms the crystalline structure of the generated silicon nanoparticles. The energy confinement of carriers which is evaluated from optical experiments varies from 90 to 550 meV when the mean nanoparticles size decreases from 60 to 2.5 nm. In particular, the evaluated nanoparticle sizes from optical analysis and the LCAO theoretical model are found in agreement with transmission electron microscopy and Raman measurements for the silicon nanoparticles with a size less than 6 nm. Finally, we present stability studies which show that the smallest nanoparticles aggregate over time.

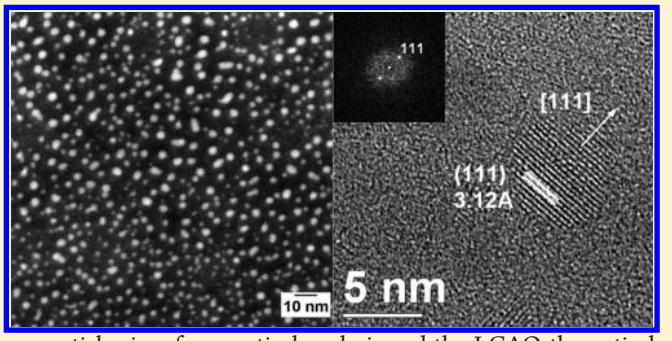

1. INTRODUCTION

Silicon nanoparticles (Si-NPs) present a growing interest due to their particular size-dependent optical properties leading to important applications such as light-emitting devices,[1] energy source,[2] and in biomedicine.[3−7] The integration of ultrathin films of Si-NPs on silicon solar cells is found to enhance the power performance of polycrystalline cells by 60% in the UV range. Recently, Si-NPs have been shown to be able to generate singlet oxygen under irradiation, making them promising candidates for photodynamic therapy. A variety of chemical[8−11] and physical[12−17] methods have been employed to prepare Si-NPs. Among them, wet chemistry routes are attractive because particle size and surface properties can be controlled simultaneously. Nevertheless, the obtained nanoparticles are contaminated with the residual byproducts such as ions and reducing agents, which is not suitable for biological application of nanoparticles. Laser ablation synthesis in liquid environment provides the advantage to reduce the risk of contamination. Biocompatibility improvement of the laser-produced nanoparticles is predicted due to their restricted surface contamination since the synthesis can be carried out in water or in solution of a biocompatible ligand, which is a key to the subsequent successful functionalization of the nanoparticle surface.[18]

There are many irradiation parameters which should be taken into account for controlling the size and shape of nanoparticles. Some of these parameters include laser wavelength, pulse energy, pulse duration, repetition rate, and liquid environments.[19−22] In particular, the laser pulse duration is found to affect directly the ablation, nucleation, growth, and aggregation mechanisms. Long laser pulses (nanosecond) release energy slowly on a time scale comparable to the thermal relaxation processes of the target, while femtosecond laser pulses release energy to electrons in the target on a time scale much faster than electron−phonon thermalization processes. Local heating on the target in this way can be reduced in the case of femtosecond pulses. Moreover, temporal overlap between laser pulse duration and the time of material evaporation induces thermodynamic instability of the plasma during this expansion.[23] Consequently, some differences are observed in the generated nanoparticles produced by means of laser with different pulse durations.[22] Only few works have been reported on generation of Si-NPs in liquid environment. Nanosecond laser ablation of silicon shows generation of nanoparticles which stabilize into clusters due to the agglomeration effect; i.e., Si-NPs are held together by an irregular network.[24−26] Strong agglomeration of the produced nanoparticles is a major barrier to most of the applications requiring nonagglomerated substrate-free nanoparticles. Recently, isolated Si-NPs have also been produced using a UV femtosecond pulse laser source.[27]

The present paper focuses on the infrared femtosecond laser ablation of silicon in deionized water aiming to clarify the possibility to get isolated Si-NPs with controllable sizes. We report the production of the Si-NPs with a mean size ranging from 60 to 2.5 nm in the absence of any reducing chemical reagents, decreasing the pulse energy value. High-resolution transmission electron microscopy (HR-TEM) together with Raman spectroscopy confirm the crystalline structure of the generated Si-NPs. The energy confinement of carriers which is

Special Issue: Laser Ablation and Nanoparticle Generation in Liquids

Received: September 29, 2010
Revised: December 14, 2010
Published: February 08, 2011

evaluated from optical experiments varies from 90 to 550 meV when the mean NP size decreases from 60 to 2.5 nm. In particular, the evaluated NP sizes from optical analysis and LCAO theoretical model are found in agreement with TEM and Raman measurements for the Si-NPs with a size less than 6 nm. Moreover, stability studies show that the smallest nanoparticles aggregate over time.

2. EXPERIMENTAL SECTION

Laser ablation experiments were carried out using a Ti:sapphire laser system providing pulses centered at 800 nm, with a maximum energy of 1 mJ/pulse at a repetition rate of 1 kHz. The laser pulses were generated by a Micra Ti:sapphire oscillator (500 mW, 80 MHz) followed by a regenerative amplifier and a compressor (Coherent's Legend Elite). The amplified laser pulses have a pulse duration of 100 fs. The target material (99.999 % Si from Alpha Aesar) in the form of a cylinder with diameter of 6 mm and thickness of 10 mm was placed on the bottom of a quartz cuvette (dimension 10 × 10 × 100 mm). The cuvette was filled with deionized water (1 mL) which corresponds to 1 cm of liquid above the surface of the target. The target was mechanically polished, and then it was washed by deionized water several times to remove impurities from the surface. The laser beam was focused below the target surface using a short focal length lens (10 cm) and kept fixed on one point of the target during all ablation. The beam diameter of 8 mm and the distance between target surface and focal plane, 5 mm, give us a estimation of the spot size, 500 μm. Pulse energies from 0.05 to 0.5 mJ were used, controlled by a set of fixed and variable attenuators. Ablation was carried out for 60 min, and the formation of NPs could be estimated by the slight change of the color of water during ablation (only at high pulse energy). All characterization measurements were performed 1 day after preparation of the colloidal solution.

Transmission electron microscopy (TEM) images were acquired on a JEOL Jem 1011 microscope working at an acceleration voltage of 100KeV. High resolution and scanning transmission electron microscopy (HRTEM and STEM, respectively) analyses were performed on a JEOL Jem 2200FS microscope equipped with a field emission electron gun working at 200 KV, and with a JED-2300 Energy Dispersive X-ray Spectrometer (EDS) and spherical aberration corrector system (Cs-corrector) for objective lens. The Cs-corrector improves the spatial resolution of the optical system that reaches the detectable spatial frequency of 0.9 Å; instead, the Z-contrast STEM measurements were acquired recording the images with a high angle annular dark field detector (HAADF) with a camera length of 50 cm. TEM/STEM samples were prepared by dropping colloidal solution directly onto a carbon-coated 300 mesh copper grids and allowing the solution to evaporate.

Microprobe Raman measurements (Jobin Yvon, model: LabRam) were excited by a 632 nm He−Ne laser (power = 3 mW and accumulation time = 20 s) in backscattering configuration with spectral resolution of about 1.1 cm^{-1}. The experimental setup consists of a grating with 600 lines/mm. The sample was deposited by a drop coating deposition (DCD) technique, in which the substance was dropped over the substrate and waited for evaporation of excess liquid. This leads to the formation of a coffee ring. To be noted, the material property of the sample in liquid and after the evaporation of excess liquid remains the same.[28] Thereafter, various measurements were performed at different positions of the coffee ring.

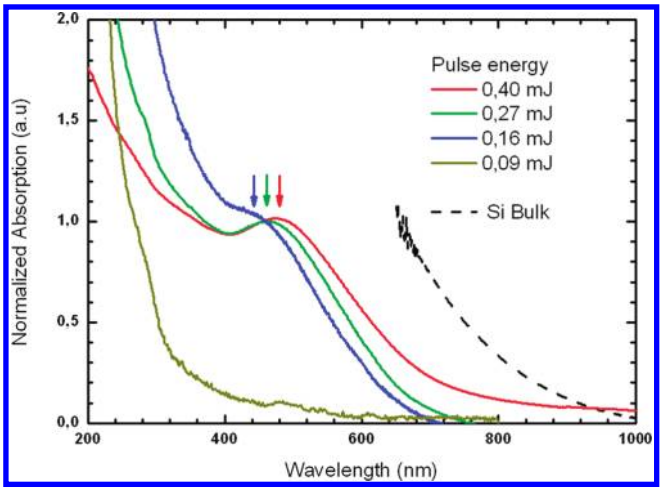

Figure 1. Absorption spectra of the Si-NPs produced via femtosecond laser ablation of a silicon target in deionized water.

Optical absorption spectra were recorded in quartz cuvette (10 mm, Helma), using a Cary 6000 UV-VIS-NIR double beam spectrophotometer. The scan range was 200−1000 nm with a 600 nm/min rate. Absorption spectra are corrected for water absorption, by subtracting the contribution of water from the recorded spectrum.

3. RESULTS

3.1. Optical Measurements. Si-NP solutions were produced by laser ablation in deionized water of a solid target, using femtosecond laser pulses emitting at 800 nm, by varying pulse energy from 0.09 to 0.40 mJ. Figure 1 shows UV−visible absorption measurements of obtained solution. All absorption spectra appear to have a broad continuous band between 200 and 800 nm and a distinctive shoulder with a minimum absorbance at around 400 nm, except for the solution obtained at lower pulse energy. For the clarity of the figure, the absorption spectra were normalized to 1 at the shoulder maximum peak value. When the pulse energy value decreases, the spectra are characterized by a blue-shift of the position of the shoulder peak together with an increase of the relative absorption intensity in the UV range. The position of the shoulder peak shifts from 480 to 440 nm. The shifting of the absorption edge is ascribed to the change in nanoparticle size which is an effect of quantum confinement (estimated in the next section).[29] The bandgap energy of Si-NPs increases (i.e., decrease of the wavelength) with reduction of their size. The UV absorption band is attributed to Si-NPs with a size varying from 1 to 3 nm, similar to the published research work on Si-NPs in the past.[8,30]

3.2. Transmission Electron Microscopy. Detailed information about the size and size distribution of the produced Si-NPs in the solution was obtained by TEM and STEM analyses. Figure 2a, Figure 2b and Figure 2c show, respectively, one TEM and two STEM images of the particles in the colloidal solution obtained by femtosecond laser ablation at different pulse energies. We can observe isolated Si-NPs (i.e., nonagglomerated substrate-free NPs) with a pseudospherical morphology and smooth surface. To be noted, SiO_x amorphous material essentially observed at higher pulse energy probably is formed during the laser ablation process (Figure 2a). Since temperature is locally high (around

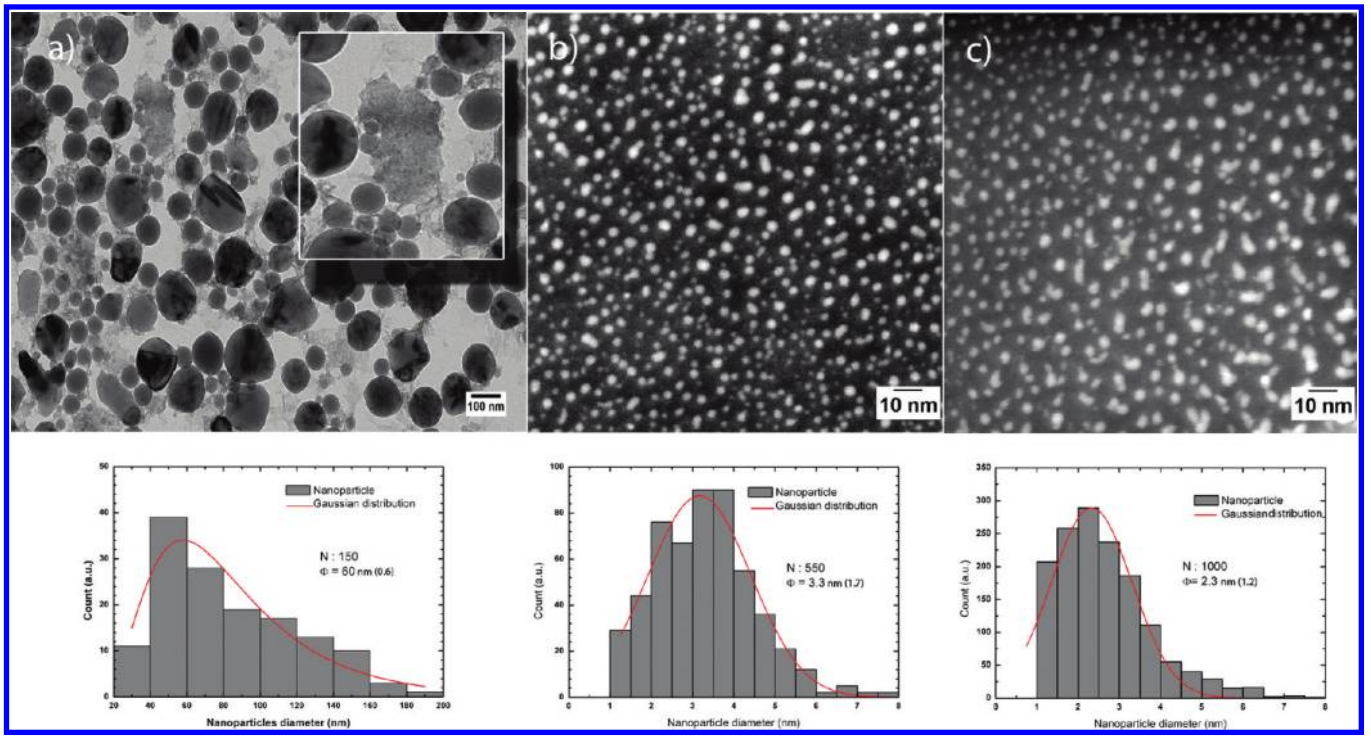

Figure 2. TEM and STEM analyses of the obtained solution by femtosecond laser ablation using different pulse energies: (a) 0.40 mJ TEM image and (b) 0.27 mJ and (c) 0.16 mJ STEM images.

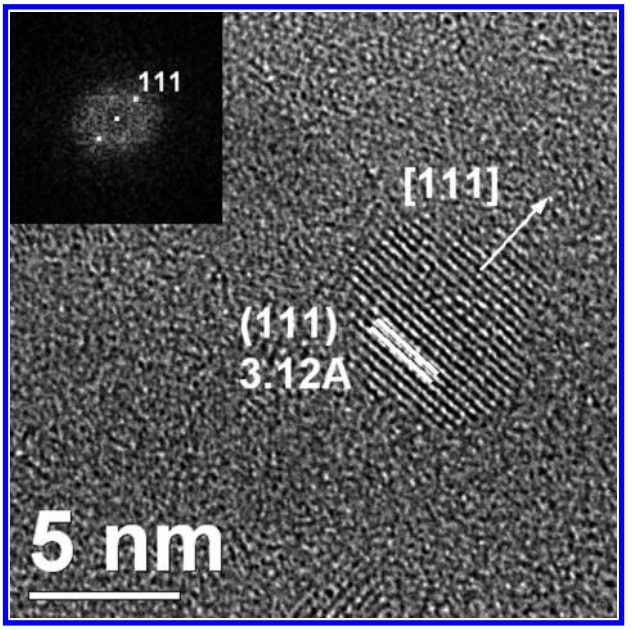

Figure 3. HRTEM image of a single synthesized Si-NP showing the (111) lattice sets and its corresponding numerical electron diffraction pattern (inset).

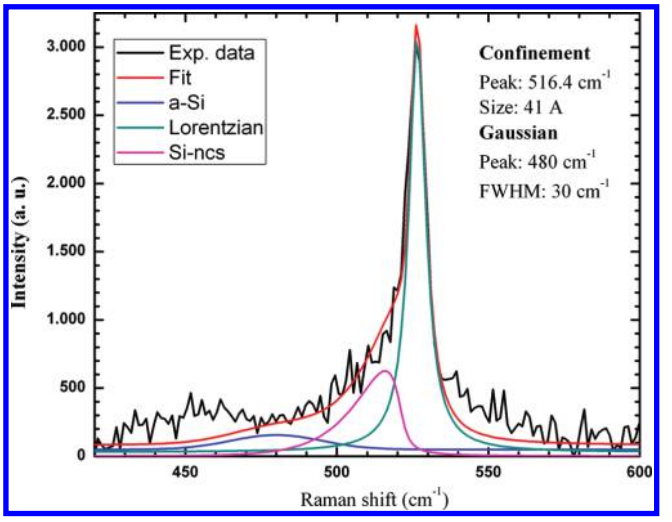

Figure 4. Raman scattering spectra of the Si-NPs synthesized via laser ablation in deionized water at a pulse energy of 0.27 mJ.

5000 K) during the laser ablation process, it is not surprising that silicon oxidation occurs when silicon and water come into contact, as observed by Sverck et al.[24] Nevertheless, contrary to nanosecond laser ablation of the silicon target,[24] the SiO_x amorphous structure is found well separated from the Si-NPs (inset of Figure 2a) and may be responsible for NPs stability, as discussed in the next section.

The mean and distribution sizes of particles obtained by counting more than 300 particles in the electron microscopy images are shown below each corresponding microphotograph. The hypothesis on the energy dependence of the NP size is confirmed and revealed a drastic particle size reduction when the pulse energy decreases. The mean particle size drops from 60 to 2.5 nm as pulse energy decreases from 0.40 to 0.16 mJ.

3.3. HR-TEM and Raman Spectroscopy. The crystallinity of the synthesized Si-NPs via laser ablation was further investigated by high-resolution transmission electron microscopy (HR-TEM image) and Raman spectroscopy. Figure 3 shows the HR-TEM of one isolated Si-NP distributed onto the carbon film. We can

observe the crystalline structure of NPs that displays the (111) lattice sets with an interplanary spacing of 3.12 Å, characteristic of Si bulk. Raman spectroscopy was performed to get an analyzed volume of the NP solution considerably higher than the one analyzed by TEM (Figure 4). The Raman spectrum shows a sharp band centered at around 520 cm^{-1} with the asymmetricity toward the lower frequency side. Asymmetricity in the Si Raman band in Figure 4 confirms the presence of Si-NPs within the sample.[31,32] This Raman shift is attributed to the quantum confinement of electronic wave function in Si-NPs and can provide the characteristic dimensions of nanocrystalline structures. The Si-NP size and the dispersion in size distribution were estimated by deconvoluting the Raman spectrum using three distribution functions: Lorentzian distribution, Phonon confinement model, proposed by Ritcher et al.[33] and modified by De Santos et al.,[34] and the Gaussian distribution function. These three independent peaks are: (i) Si sharp peak in the vicinity of 520 cm^{-1} (bulk Si having crystalline size >9 nm); (ii) an intermediate peak between 510 and 520 cm^{-1} originating from relatively small Si crystallites (i.e., Si-NPs), estimated after fitting the peak using phonon confinement model; and (iii) an amorphous Si peak at approximately 480 cm^{-1}.[35] Si-NP size is found to be around 41 A with the size dispersion of 1 A, in agreement with the STEM image (Figure 2b). The Raman peak in the vicinity of 520 cm^{-1} indicates the presence of crystalline Si with the grain size higher than 9 nm. Nevertheless, the STEM images and the histograms originating from their analysis shown in Figure 2 demonstrate that the vast majority of the produced NPs have very small average sizes (~ 4 nm) but that a small percentage of larger NPs are always present due to the particularity of the laser synthesis.

3.4. Optical Analysis. Si-NPs generated so far by laser ablation (using long pulse) or with other methods were confirmed to be indirect band gap semiconductors.[25,36] The data in Figure 5 have been plotted as $\alpha(\omega)^{1/2}$ as a function of the photon energy $\hbar\omega$. In such plots, linear behavior is expected for semiconductors with an indirect band gap, for which one expects an energy dependence of the fundamental absorption as given by $\alpha(\hbar\omega) \propto \omega^{-1}(\hbar\omega - E_g)^2$. As we can see from Figure 5, the absorption spectra in such plots show linear behavior, except for

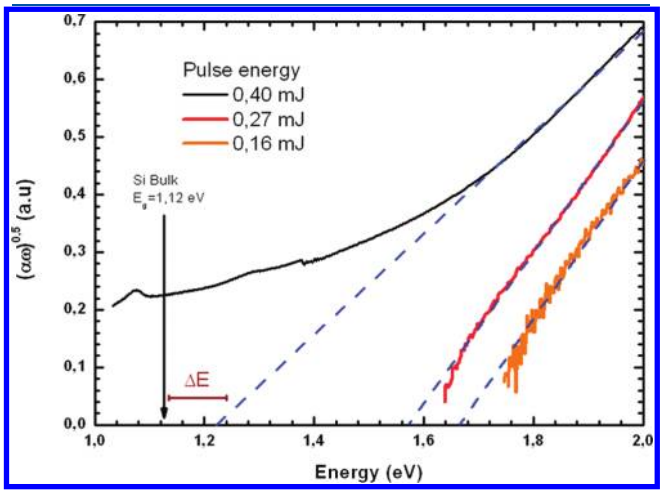

Figure 5. Absorption data for Si-NPs synthesized via femtosecond laser ablation of the silicon target in deionized water at different pulse energies, plotted as $\alpha(\omega)^{1/2}$ vs $(\hbar\omega)$, corresponding to an indirect semiconductor. Dashed lines, extrapolation for determination of the electronic band gap.

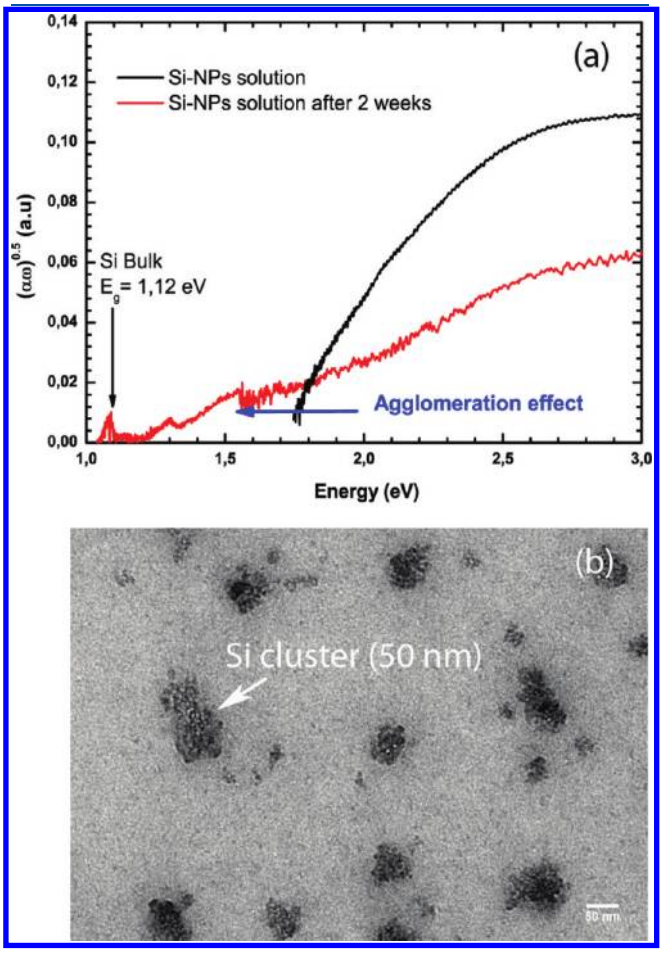

Figure 6. (a) Absorption spectra of Si-NPs in deionized water as synthesized (black line), after 15 days (red line), plotted as $\alpha(\omega)^{1/2}$ vs $(\hbar\omega)$. (b) TEM image of the Si-NP solution after 15 days. The agglomeration effect is clearly observed by the formation of a cluster with a size around 50 nm, having bulk properties.

Table 1. Si-NP Parameters Obtained from TEM and Absorption Spectroscopy[a]

pulse energy (mJ)	E_g(NPs) (eV)	ΔE (meV)	$D(\mathrm{NPs})_{\mathrm{TEM}}$ (nm) (σ)	$D(\mathrm{NPs})_{\mathrm{abs}}$ (nm)
0.16	1.67 ± 0.01	550 ± 20	2.5 (1.2)	3.96 ± 0.1
0.27	1.56 ± 0.01	440 ± 20	3.5 (1.7)	4.65 ± 0.2
0.40	1.21 ± 0.01	90 ± 20	60 (0.6)	14.5 ± 3

[a] E_g(NPs) corresponds to the experimental value of NP band gap obtained by absorption analysis. ΔE corresponds to the quantum energy confinement and experimental error (including error linear fit), 20 meV. $D(\mathrm{NPs})_{\mathrm{TEM}}$ corresponds to the NP mean size obtained by TEM analysis. σ corresponds to the standard deviation. $D(\mathrm{NPs})_{\mathrm{Abs}}$ corresponds to the calculated NP size from absorption measurements (ΔE) and empirical law, $\Delta E = \pi\beta/(D^{\gamma})$. Model uncertainty is reported.

dx.doi.org/10.1021/jp109351t |J. Phys. Chem. C 2011, 115, 5102–5107

the Si-NPs of bigger size. The observed shift can be due to the effect of particle size distribution as observed in the TEM image and/or SiO_x amorphous absorption structure.[37] The band gap energy of the obtained NP solution has been determined using linear approximation of the previous relation, as shown in Figure 5, and consequently the NP quantum energy confinement, ΔE. To validate the accuracy of our method, we have used the known electronic band gap of bulk silicon, $E_g = (1.12 \pm 0.01$ eV). Therefore, we assume that the method has an experimental inaccuracy ΔE of 20 meV, including the linear fit error. The value of the band gap energy and the quantum energy confinement (ΔE) of the obtained NPs solution are reported in Table 1. It is possible to estimate the Si-NP size from ΔE, using the empirical law $E_g(d) = E_{g0} + \pi\beta/(D^\gamma)$. β and γ depend on the nature of the surface as well as size and symmetry of NPs, and D corresponds to NP size. For the NP size estimation, we used the values (β = 3.73, γ = 1.39) which have been calculated by Delarue et al. for relatively small spherical Si-NPs (<10 nm) using a linear combination of atomic orbitals (LCAO).[30] It can be seen in Table 1 that the NP diameter determined from the optical experiments is in agreement with the NP diameter obtained by TEM analysis for smaller NPs, while the diameter is underestimated for larger NPs. One has to take into account that the analyzed volume of the NP solution from absorption spectroscopy is considerably higher than the one of TEM. For NPs below 5 nm, the difference in size is obviously caused by the particle size distribution, in which particles substantially larger than the mean particle size observed in the STEM image (Figure 2b) always contribute to the absorption, thus increasing the calculated NP diameter. For a NP population of bigger size, several factors can influence the accuracy of the calculated NP size determinate from optical experiments and the LCAO theoretical model: (i) From a theoretical model point of view (β = 3.73, γ = 1.39), parameters have been calculated by Delerue et al., for a population of NPs less than 10 nm and could be not available for bigger NPs. (ii) The estimated mean size from a STEM image analysis histogram (Figure 2b) can be misleading since it is not possible to analyze all the TEM grid surface and consequently all the NPs solutions; i.e., the density of NPs with a size around 20 nm could be higher than those observed in the acquired electron microscopy photographs. (iii) Finally, it is known that the surroundings of the NPs (Figure 2a) and, consequently, the chemical nature of the NP surface can affect the optical properties of NP solutions, i.e., quantum confinement.[38−40]

4. STABILITY OF NANOPARTICLE SOLUTION: AGING EFFECT

The aging of NP solution leading to aggregation is known to be directly linked to the chemical nature of the NP surface. In this section, we report the agglomeration effect of the Si-NPs obtained at different pulse energy values (i.e., different NP size) in deionized water. The Si-NP solution of bigger size (i.e., obtained at higher pulse energy) did not show any sign of agglomeration within several months after the preparation. The stability could be attributed to the presence of a surface oxide layer[41,42] as observed in TEM images (Figure 2a). In contrary, the Si-NPs produced at lower pulse energy (size less than 10 nm) are found to be less stable, indicating a different chemical nature of the NP surface. In Figure 6a is reported the absorption spectra of the NP solution with size less than 4 nm, performed just after the synthesis and after 2 weeks. The absorption edge is found to shift to lower energy, exhibiting the features associated to Si bulk materials. This observation is characteristic of an agglomeration effect of the Si-NPs and can be understood in terms of an evolution from isolated (localized) NPs to collective electronic states delocalized within a finite number of NPs.[43] TEM analyses of the aged Si-NPs solution are also reported in Figure 6b. We can observe aggregates with a size around 50 nm composed of nanospheres, in agreement with the optical measurements.

5. CONCLUSIONS

Ultrafast laser ablation of a Si target in deionized warter was employed to prepare size-controlled silicon nanoparticles in solution. Contrary to nanosecond laser ablation of the silicon target, the SiO_x amorphous structure is found well separated from the silicon nanoparticles. We obtain isolated Si-NPs (i.e., nonagglomerated substrate-free nanoparticles) with pseudospherical morphology and smooth surface. The mean size is found to vary from 60 to 2.5 nm in the absence of any reducing chemical reagents, decreasing the pulse energy value. The crystalline structure of the generated silicon nanoparticles has been confirmed by high-resolution transmission electron microscopy and raman spectroscopy. The energy confinement of carriers evaluated from optical experiments varies from 90 to 550 meV when the mean NP size decreases from 60 to 2.5 nm. In particular, the evaluated NP size from optical analysis and LCAO theoretical model are found in agreement with TEM and Raman measurements for the Si-NPs with a size less than 6 nm. Finally, stability studies show that the smallest nanoparticles aggregate over time.

AUTHOR INFORMATION

Corresponding Author
*E-mail: romuald.intartaglia@iit.it.

ACKNOWLEDGMENT

This work was supported by the Italian Institute of Technology. The authors gratefully acknowledge the technical help of Marco Scotto d' Abbusco.

REFERENCES

(1) Walters, R. J.; Bourianoff, G. I.; Atwater, H. A. *Nat. Mater.* **2005**, *4*, 143–146.
(2) Stupca, M.; Alsalhi, M.; Al Saud, T.; Almuhanna, A.; Nayfeh, M. H. *Appl. Phys. Lett.* **2007**, *6*.
(3) Wang, G.; Yau, S. T.; Mantey, K.; Nayfeh, M. H. *Opt. Commun.* **2008**, *281*, 1765–1770.
(4) Gross, E.; Kovalev, D.; Kunzner, N.; Diener, J.; Koch, F.; Timoshenko, V.Yu.; Fujii, M. *Phys. Rev. B* **2003**, *68*, 115405.
(5) Rioux, D.; Laferrière, M.; Douplik, A.; Shah, D.; Lilge, L.; Kabashin, A. V.; Meunier, M. J. *Biomed. Opt.* **2009**, *14*, 021010.
(6) Gaspari, M.; Cheng, M. M.-C.; Terracciano, R.; Liu, X.; Nijdam, A. J.; Vaccari, L.; Di Fabrizio, E.; Petricoin, E. F.; Liotta, L. A.; Cuda, G.; Venuta, S.; Ferrari, M. *Journal of Proteome Research.* **2006**, *5* (5), 1261–1266.
(7) De Angelis, F.; Pujia, A.; Falcone, C.; Iaccino, E.; Palmieri, C.; Liberale, C.; Mecarini, F.; Candeloro, P.; Luberto, L.; De Laurentiis, A.; Das, G.; Scala, G.; Di Fabrizio, E. *Nanoscale* **2010**, *2*, 2230–2236.
(8) Rosso-Vasic, M.; Spruijt, E.; Popovic, Z.; Overgaag, K.; Van Lagen, B.; Grandidier, B.; Vanmaekelbergh, D.; Dominguez-Gutierrez, D.; De Cola, L.; Zuilhof, H. *J. Mater. Chem* **2009**, *19*, 5926–5933.

(9) Arul Dhas, N.; Paul Raj, C.; Gedanken, A. *Chem. Mater.* **1998**, *10*, 3278–3281.
(10) Zhang, X.; Neiner, D.; Wang, S.; Louie, A. V.; Kauzlarich, S. M. *Nanotechnology* **2007**, *18*, 095601.
(11) Warner, J. H.; Rubinsztein-Dunlop, H.; Tilley, R. D. *J. Phys. Chem. B* **2005**, *109* (No. 41), 19064–19067.
(12) Soni, R. K.; Fonseca, L. F.; Resto, O.; Buzaianu, M.; Weisz, S. Z. *J. Lumin.* **1999**, *83−84*, 187–191.
(13) Riabinina, D.; Durand, C.; Chaker, M.; Rosei, F. *Appl. Phys. Lett.* **2006**, *88*, 073105.
(14) Smirani, R.; Martin, F.; Abel, G.; Wang, Y. Q.; Ross, G. G. *Nanotechnology* **2005**, *16*, 32–36.
(15) Wu, M. H.; Mu, R.; Ueda, A.; Henderson, D. O.; Vlahovic, B. *Mater. Sci. Eng., B* **2005**, *116*, 273–277.
(16) Kabashin, A. V.; Sylvestre, J. P.; Patskovsky, S.; Meunier, M. *J. Appl. Phys.* **2002**, *91* (No. 5), 3248–3254.
(17) Knipping, J.; Wiggers, H.; Rellinghaus, B.; Roth, P.; Konjhodzic, D.; Meier, C. *J. Nanosci. Nanotechnol.* **2004**, *4* (No. 8), 1039–1044.
(18) Kabashin, A. V.; Meunier, M. *Laser Ablation-Based Synthesis of Nanomaterials, in Recent Advances in Laser Processing of Materials*; Fogarassy, E., Ed.; Elsevier: Oxford, 2006.
(19) Tsuji, T.; Iryo, K.; Watanabe, N.; Tsuji, M. *App. Surf. Sci.* **2002**, *202*, 80–85.
(20) Mafune, F.; Kohno, J.; Takeda, Y.; Kondow, T.; Sawabe, H. *J. Phys. Chem. B* **2000**, *104*, 9111–9117.
(21) Shafeev, G. A.; Freysz, E.; Bozon-Verduraz, F. *Appl. Phys. A: Mater. Sci. Process.* **2004**, *78*, 307–309.
(22) Tsuji, T.; Kakita, T.; Tsuji, M. *Appl. Surf. Sci.* **2003**, *206*, 314–320.
(23) Amendola, V.; Meneghetti, M. *Phys. Chem. Chem. Phys.* **2009**, *11*, 3805–3821.
(24) Švrček, V.; Mariotti, D.; Kondo, M. *Opt. Express* **2009**, *17* (Iss. 2), 520–527.
(25) Umezu, I.; Minami, H.; Senoo, H.; Sugimura, A. *J. Phys.: Conf. Ser.* **2007**, *59*, 392–395.
(26) Švrček, V.; Sasaki, T.; Shimizu, Y.; Koshizaki, N. *J. Laser Micro/Nanoeng.* **2007**, *2* (No. 1), 15–20.
(27) Semaltianos, N. G.; Logothetidis, S.; Perrie, W.; Romani, S.; Potter, R. J.; Edwardson, S. P.; French, P.; Sharp, M.; Dearden, G.; Watkins, K. G. *J. Nanopart. Res.* **2009**, *12* (No. 2), 573–580.
(28) Pelletier, M. J.; Altkorn, R. *Anal. Chem.* **2001**, *73*, 1393–1397.
(29) Kovalev, D.; Heckler, H.; Polisski, G.; Koch, F. *Phys. Status Solidi* **1999**, *215*, 871–932.
(30) Delerue, C.; Allan, G.; Lannoo, M. *Phys. Rev. B* **1993**, *48*, 11024–11036.
(31) Mariotto, G.; Das, G.; Quaranta, A.; Della Mea, G.; Corni, F.; Tonini, R. *J. Appl. Phys.* **2005**, *97*, 113502.
(32) Arguirov, T.; Mchedlidze, T.; Akhmetov, V. D.; Kouteva-Arguirova, S.; Kittler, M.; Rolver, R.; Berghoff, B.; Forst, M.; Batzner, D. L.; Spangenberg, B. *Appl. Surf. Sci.* **2007**, *254* (4), 1083–1086.
(33) Richter, H.; Wang, Z. P.; Ley, L. *Solid State Commun.* **1981**, *39* (5), 625–629.
(34) Dos Santos, D. R.; Torriani, I. L. *Solid State Commun.* **1993**, *85* (4), 307–310.
(35) Mchedlidze, T.; Arguirov, T.; Kouteva-Arguirova, S.; Kittler, M.; Rölver, R.; Berghoff, B.; Bätzner, D. L.; Spangenberg, B. *Phys. Rev. B* **2008**, *77*, 161304(R).
(36) Meier, C.; Gondorf, A.; Lüttjohann, S.; Lorke, A.; Wiggers, H. *J. Appl. Phys.* **2007**, *101*, 103112.
(37) Tan, G. L.; Lemon, M. F.; French, R. H. *J. Am. Ceram. Soc.* **2003**, *86* (11), 1885–92.
(38) Ledoux, G.; Guillois, O.; Porterat, D.; Reynaud, C.; Huisken, F.; Kohn, B.; Paillard, V. *Phys. Rev. B* **2000**, *62* (No.23), 15942–15951.
(39) Warner, J. H.; Rubinsztein-Dunlop, H.; Tilley, R. D. *J. Phys. Chem. B* **2005**, *109* (41), 19064–19067.
(40) Salivati, N.; Shuall, N.; McCrate, J. M.; Ekerdt, J. G. *J. Phys. Chem. Lett.* **2010**, *1* (13), 1957–1961.
(41) Bley, R. A.; Kauzlarich, S. M.; Davis, J. E.; Lee, H. W. H. *Chem. Mater.* **1996**, *8* (8), 1881–1888.
(42) Papadimitrakopoulos, F.; Wisniecki, P.; Bhagwagar, D. E. *Chem. Mater.* **1997**, *9* (12), 2928–2933.
(43) Artemyev, M. V.; Bibik, A. I.; Gurinovich, L. I.; Gaponenko, S. V.; Woggon, U. *Phys. Rev. B* **1999**, *60*, 1504–1506.